ARTICLES

Optical Properties of Platinum-Coated Gold Nanorods

Marek Grzelczak,[†] Jorge Pérez-Juste,[†] F. Javier García de Abajo,[‡] and Luis M. Liz-Marzán*[,†]

Departamento de Química Física and Unidad Asociada CSIC, Universidade de Vigo, 36310 Vigo, Spain, and Instituto de Óptica, CSIC, Serrano 121, 28006 Madrid, Spain

Received: October 31, 2006; In Final Form: January 11, 2007

The optical properties of Au/Pt nanorods with different morphologies are analyzed in detail through comparison of experimental UV−vis−NIR spectra and calculations based on the boundary element method (BEM). The studied morphologies refer to two different Pt deposition modes on Au nanorods, which have been experimentally realized through the presence or absence of Ag^+ ions in solution. While in the absence of Ag^+, complete overcoating was obtained, the presence of these ions induced preferential growth on the tips, as recently reported by us.[1] The changes in the optical spectra are different for both Pt deposition modes, and this is fully accounted for using appropriate geometrical models in the BEM calculations. The presence of Pt tips is shown to lead to red-shifts of the longitudinal plasmon band because of geometrical effects, though accompanied by damping due to increased absorption.

1. Introduction

The optical properties of metal nanoparticles are dominated by surface plasmon resonances (i.e., collective oscillations of conduction electrons in phase with an external electromagnetic wave).[2] The resonance frequency can be modulated through the composition, size, shape, and electromagnetic environment of the metal particles.[3,4] Because of the large interest from both the scientific and technological points of view, the research on such metallic nanostructures has been tremendously intense during the past couple of decades. Although initially only spherical nanoparticles were investigated, it was soon realized that anisotropy effects were much more dramatic than those derived from size and even composition. Therefore, research on metal nanorods,[5] nanowires,[6] nanocubes,[7] nanoprisms,[8,9] or even nanostars[10] has demonstrated that small variations in the morphology of the particles could strongly influence the optical response. In the case of small gold nanorods, two plasmon resonances are possible, which are associated to conduction−electron oscillations parallel (longitudinal plasmon band, LPB) and perpendicular (transverse plasmon band, TPB) to the rod long axis, with the LPB being much more sensitive to the nanorod aspect ratio (length/width) than the TPB.[11] Some examples have been shown in which manipulation of the plasmon resonances of Au nanorods was achieved through deposition of different materials, such as Ag,[12−14] Ag_2S, Ag_2Se,[15] or SiO_2.[16,17] In all these examples, the deposited material covers completely the core Au rods so that the observed effects arise mainly from the variation of the immediate dielectric environment around them. However, in the context of adding a catalytic functionality to optically active nanorods, we have recently reported[1] that the growth of platinum shells on gold nanorods can take place in two different ways, depending on whether a small amount of Ag^+ ions is present or not in the growth solution, so that in the absence of Ag^+ complete coverage is achieved, while in the presence of Ag^+ tip-coating is strongly enhanced. In the same paper, preliminary results on the optical effects derived from the two different growth modes were shown, though with a purely qualitative description.

In this paper, we present a detailed theoretical modeling based on the boundary element method (BEM),[18,19] which has been recently shown to agree well with experimental results for Au nanodecahedra.[20] In the BEM, the induced electric and magnetic fields are viewed as originating from equivalent boundary sources (i.e., equivalent surface electric charges and currents), which are used to fulfill the customary boundary conditions of the electromagnetic field at the interfaces between different media. The surface integrals are then discretized by means of boundary elements, thus yielding a linear system of equations that are solved numerically. This is a rigorous approach to solve Maxwell's equations with extremely good convergence with respect to the number of boundary elements. The latter increases quadratically with the size of the particle because only surface boundaries between different media need to be parametrized. This results in a relatively modest computational demand that allows us to directly solve the entire linear algebra problem by direct matrix inversion. By contrast, other methods based upon discretization of the entire volume occupied by the particle require a number of volume elements that scales with the cube of the particle size. This is the case of the discrete-dipole approximation (DDA) that can be accelerated at the expense of accuracy by recasting the real-space problem in momentum space.[21] Finite-difference in the time domain (FDTD) methods[22] suffer from an even more dramatic increase in computational demand because they rely on parametrization of the entire volume outside and inside the particle. In the present study,

* Corresponding author. E-mail: lmarzan@uvigo.es.
[†] Universidade de Vigo.
[‡] CSIC.

10.1021/jp0671502 CCC: $37.00
Published on Web 04/11/2007

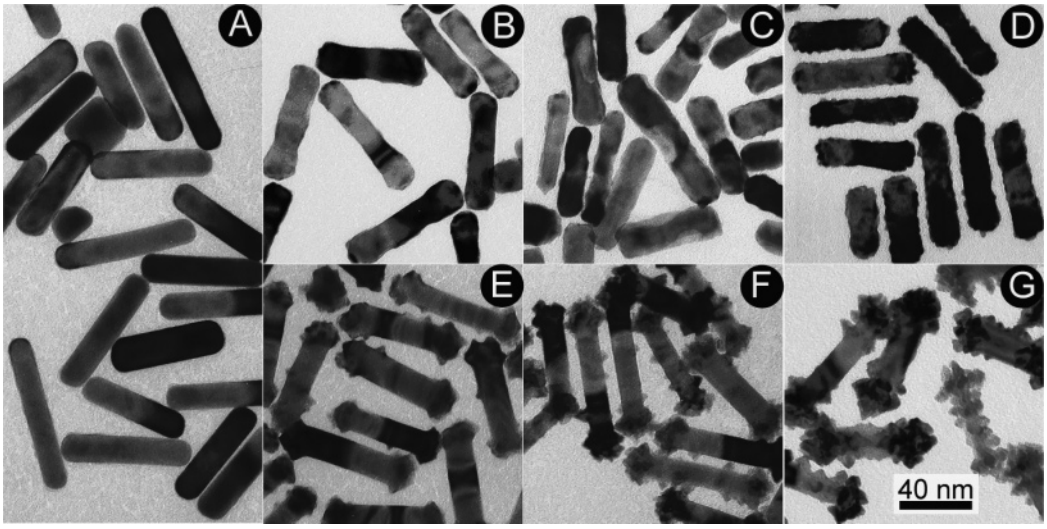

Figure 1. TEM micrographs show gold nanorods before platinum deposition (A) and Pt overcoated (B−D) and tip-coated (E−G). The amount of platinum with respect to gold was varied between 20 (B,E), 40 (C,F), and 100 mol % (D,G).

the axial symmetry of the particles is utilized to reduce the computational size of the problem to one dimension (the radial contour of the particle with respect to the axis of rotation). Further details on the calculation method are provided in the experimental section. Our calculated results for geometrical models devised on the basis of the nanoparticle morphologies observed in the transmission electron microscopy (TEM) images show very good agreement with measured optical spectra and allow us addressing questions such as the symmetry and the near-field enhancement associated to the particle surface plasmons observed through absorption bands.

2. Experimental Methods

Gold Nanorods Synthesis and Platinum Deposition. The details of the synthesis have been thoroughly described in ref. 1. Briefly, Au nanorods were prepared through a seeding growth method originally developed by Nikoobakht and El-Sayed[23] and modified by Liu and Guyot-Sionnest.[24] The rods used had an average length of 59.0 nm and average width of 15.4 nm, resulting in an average aspect ratio of 3.9. Platinum growth was carried out in two different ways (in the absence and in the presence of silver ions). For platinum deposition in the absence of Ag^+, 5 mL of 0.48 mM as-prepared Au nanorods were centrifuged (8500 rpm, 10 min) to remove remaining Ag^+ ions from solution, and were redispersed in 0.1 M CTAB (10 mL). To 5 mL of 0.157 mM washed gold nanorods was added 78.5 μL of 0.01 M K_2PtCl_4 at 40 °C and was left for 30 min to allow for complexation of the platinum salt with CTAB, followed by the addition of 157 μL of 0.1 M ascorbic acid, maintaining the temperature at 40 °C for 12 h to ensure complete reduction. Pt-coated Au (Au@Pt) nanorods were washed three times by centrifugation (8500 rpm, 10 min) and were redispersed in 0.1 M CTAB.

In the case of platinum deposition in the presence of Ag^+, 10 mL of 0.1M CTAB was added to 5 mL of 0.48 mM as-prepared gold nanorods in CTAB solution, followed by reduction of platinum, and washing as described for the Ag^+-free overgrowth process.

Characterization Techniques. Optical characterization was carried out by UV−vis−NIR spectroscopy on a Cary 5000 UV−vis−NIR spectrophotometer, using 1 mm path length quartz cuvettes. TEM images were obtained with a JEOL JEM 1010 transmission electron microscope operating at an acceleration voltage of 100 kV. A more complete characterization can be found in ref. 1.

Optical Modeling. Simulation of optical spectra was based on the BEM. In the BEM, scalar and vector potentials ϕ and $\mathbf{A}$ are used, and they are expressed inside each homogeneous region of space as the sum of an external field contribution (i.e., the potentials corresponding to the incident light plane wave for which the scalar potential can be chosen as zero) and surface integrals involving the noted equivalent boundary charges σ_j and currents $\mathbf{h}_j$, defined on the boundary of region j, denoted S_j. In our case, $j = 1$, 2, and 3 label water (index of refraction taken constant and equal to 1.333, the value at 600 nm), platinum, and gold (tabulated frequency-dependent dielectric functions taken from optical measurements for platinum[25] and gold,[26] respectively). For $\mathbf{r}$ inside medium j, one has $\phi(\mathbf{r}) = \int_{S_j} d\mathbf{s} G_j(|\mathbf{r} - \mathbf{s}|)\sigma_j(\mathbf{s})$ and $\mathbf{A}(\mathbf{r}) = \mathbf{A}^{ext}(\mathbf{r}) + \int_{S_j} d\mathbf{s} G_j(|\mathbf{r} - \mathbf{s}|)\mathbf{h}_j(\mathbf{s})$, where $G_j(|\mathbf{r} - \mathbf{s}|) = (e^{ikj|\mathbf{r}-\mathbf{s}|}/|\mathbf{r} - \mathbf{s}|)$ takes care of the propagation of the electromagnetic signal in medium j; $k_j = (\omega/c)\sqrt{\epsilon_j}$ is the momentum of light inside medium j of dielectric function $\epsilon_j(\omega)$ and $\mathbf{A}^{ext}$ is the vector potential associated to the incoming light, which is nonvanishing only for $j = 1$ (i.e., in the medium outside the particle). The boundary conditions of the electromagnetic field are then imposed and yield a set of self-consistent surface integral equations that determine the boundary sources and that are solved by discretizing the boundaries through a finite number of representative points. This leads to a linear set of equations that can be solved by linear algebra techniques.[18,19] The particles were described by axially symmetric shapes capturing the main physical aspects of their response to external illumination. The BEM is particularly advantageous in axial symmetry in which different azimuthal components m that depend on the azimuthal angle ϕ as $e^{im\phi}$ are uncoupled. Then, the surface of the particle can be parametrized with a contour line thus reducing the problem effectively to one dimension. We have devised geometrical models based on the shape of the Au/Pt composite nanoparticles observed in the TEM images at various stages during both growth modes, as detailed below. The circular edges are rounded to avoid sharp corners that can cause numerical problems.[27] Convergence to the point in which differences in numerical results cannot be resolved on the scale of the figures when changing the number of parametrization points N has been achieved for $N \approx 200$, except in tip-coated particles, which

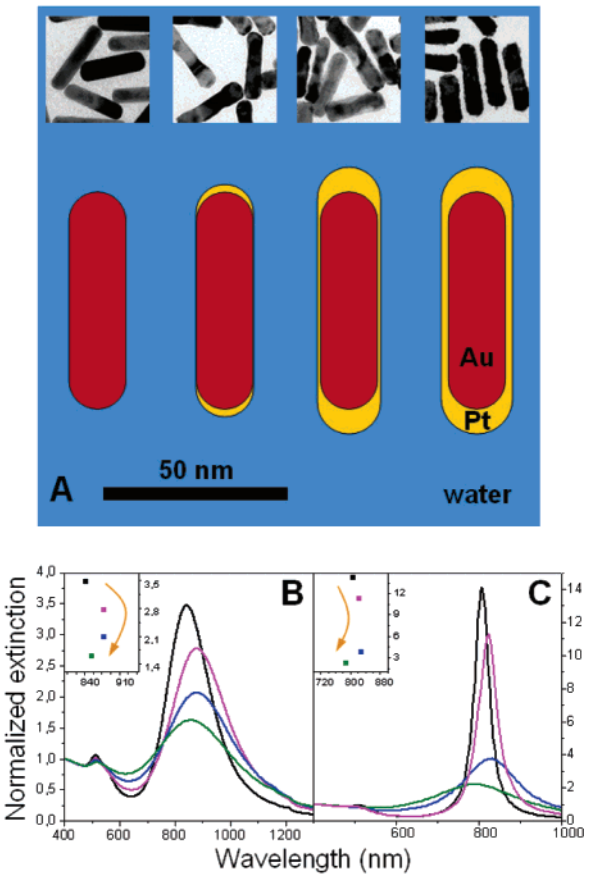

Figure 2. (A) Geometrical-capped cylinder models for Pt-coated Au rods and the corresponding TEM images before (left) and after deposition (in the absence of Ag^+) of various amounts of platinum: 20, 40, and 100 mol % (from left to right). **(**B,C**)** Measured (B) and calculated (C) UV−vis−NIR spectra of the particles shown in (A). The dominant absorption band shifts in the direction of the arrow shown in the insets as more Pt is added.

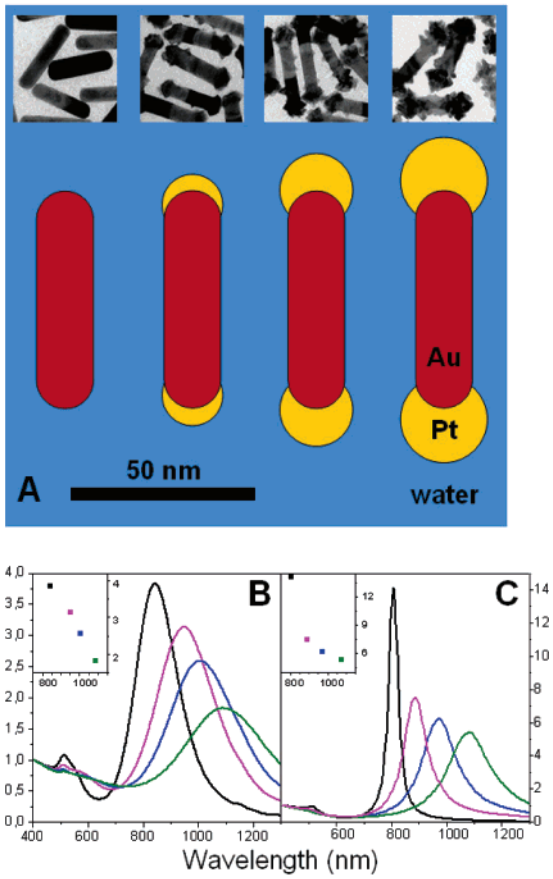

Figure 3. (A) Geometrical-capped cylinder models for Au rods with Pt tips and the corresponding TEM images before (left) and after deposition of various amounts of platinum: 20, 40, and 100 mol % in the presence of Ag^+ (from left to right). (B,C) Measured (B) and calculated (C) UV−vis-NIR spectra of the particles shown in (A). The absorption band red-shifts as more Pt is added.

required a larger number of points due to the boundary-crossing point separating Au, Pt, and water. This degree of convergence shows the robustness of the BEM, as compared to other methods such as FDTD, where the extreme computational demand prohibits similar accuracy.

3. Results and Discussion

As we have recently demonstrated,[1] the growth of platinum shells on gold nanorods can take place according to two differentmechanisms, the key factor being the presence or absence of silver cations. For the platinum deposition on the nanorods in the absence of Ag^+ (see Figure 1,B−D), we proposed an electric-field-directed mechanism in which $PtCl_4^{2-}$ ions are complexed to CTAB micelles and get reduced by ascorbic acid on the surface of gold nanorods. The different curvatures available in the rodlike gold particles lead to a faster potential decay from the tips than from the sides[28] and this makes deposition start on the tips. However, when the amount of platinum salt is increased with respect to Au^0 concentration, the collision frequency between $PtCl_4^{2-}$−CTAB micelles and gold nanorods increases, resulting in smooth coverage of the gold nanorods with platinum. On the other hand, in the presence of Ag^+ (Figure 1,E−G) the underpotential deposition mechanism (UPD)[24] is more plausible, by which Ag^+ gets reduced to Ag^0 at the gold rod surface with a lower surface potential than the bulk reduction potential of Ag^+. Electrochemical and crystallographic studies have shown that at the tips of gold nanorods Au−Ag energy binding is lower that on the side, and thus when the $PtCl_4^{2-}$−CTAB complexes approach the gold nanorod surface, reduction at the sides is hindered and tip-coating is the most favorable mechanism. When larger amounts of platinum are used (above 100 mol %), the collision frequency between $PtCl_4^{2-}$−CTAB micelles and nanoparticles should increase and oxidation of silver can occur not only at the tips but also on the edges.

For both deposition mechanisms, platinum reduction starts preferentially at the tips, but tip deposition can either continue (with Ag^+) or lead to complete overcoating (no Ag^+), which is confirmed by TEM observation (Figure 1). As was preliminarily reported,[1] the different deposition modes have also different effects on the optical (surface plasmon) response of the nanorod dispersions, which is reflected in the corresponding UV−vis−NIR spectra (see Figures 2B and 3B). Summarizing, for the overcoating model strong damping of the LPB is observed but with only small variations in the resonance frequency, while for the tip-coating model a similar damping occurs but is accompanied by a strong red-shift of the LPB. These effects seem to be related to the interband transitions in platinum, which contribute to LPB broadening, as well as the relative changes in the nanorod shape and aspect ratio during deposition, which give rise to resonance shifts, as well as to new tip-bound resonances in the case of tip-coated particles. However, detailed modeling was required to fully understand this behavior.

For such accurate simulation of the optical properties of gold nanorods coated with platinum, it is mandatory to choose a

suitable geometric model. Although traditionally the Mie−Gans theory for prolate ellipsoids[29] was used for the modeling of Au nanorods, TEM consistently shows that the geometry of the rods is closer to spherically capped cylinders. This has been recently investigated by Kooij et al.[30] through a comparison between ellipsoid and cylinder models for the accurate position of the LPB. The reported results indicate that although both the cylinder and the ellipsoid have a circular cross-section perpendicular to the long axis, the cylinder has relatively more matter at the ends of the nanorod as compared to the ellipsoid, and hence it has a larger "effective" aspect ratio. In the present case, a correct account of the nanorod tips was crucial to understand the effect of platinum deposition, and thus the cylinder model is clearly more appropriate than the ellipsoid model. However, again using the TEM images as the model, we and others[23,24,31] consistently observed that the tips are not flat (as in an ideal cylinder) but display a certain curvature (see Figure 1A), which we tried to incorporate in the model through hemiellipsoidal caps, with an aspect ratio[32] of 3.9, which is the average determined from TEM images.

In ref 30, the calculations were carried out using the DDA.[21] However, the authors explicitly indicate in the introduction the drawbacks of using this model for small metallic structures, which imply very long computational times. For this reason, in this work we have carried out all calculations using the BEM, which is computationally much more efficient, as has been indicated in the introduction.

In accordance with the two different growth modes observed experimentally and on the basis of dimensions measured from TEM images,[1] we devised two geometrical morphologies for the calculations. To account for the overcoating model (Pt deposition in the absence of Ag^+), we assumed initial tip-coating, followed by overcoating, but still with a relatively faster growth at the tips, as schematically indicated in Figure 2A. The capped-cylinder model used for simulation of UV−vis spectra had a total length (including the hemiellipsoidal caps) of 59.0 nm and a width of 15.4 nm, resulting in an aspect ratio of 3.9. For each deposition process (with or without Ag^+), the Pt/Au molar ratio was varied between 20 and 100 mol % (the amount of Au^0 was determined from the absorbance at 400 nm). For the smaller amount of Pt deposited (20 mol%), we assumed an Au-capped cylinder coated with Pt only on the tips, as sketched in Figure 2A. For 40% Pt, the thickness on the tips increases and a thin layer is considered on the lateral edges, while for 100% Pt, only the Pt thickness on the edges was increased. By using these geometrical models and averaging over 50 different orientations, complete UV−vis spectra could be calculated (Figure 2C) and compared with the corresponding experimental spectra for the particles dispersed in water (Figure 2B). Although the calculated spectra show much stronger damping (due in part to finite size distribution in the particle population), the tendency in the peak position is precisely the same with an initial red-shift for low-Pt content (20 mol %), presumably due to the increase in aspect ratio, followed by a blue-shift for larger amounts of deposited Pt, because then it gets closer to the response of a pure Pt nanorod (broad and strongly blue-shifted LPB, because of less negative values of the real part of the permittivity, as compared to Au), as summarized in the insets of Figure 2B,C. It should be stressed that the initial red-shift for low-Pt content can only be explained with the initial preferential growth on the tips, because overcoating with a thin shell (data not shown) would readily lead to strong damping and blue-shift.

One might think that the rough morphology of the shells observed in the case of tip-coating makes the modeling more complicated. However, this local roughness is not expected to have a marked influence on the far field response, and for this reason we used a simple model based on the deposition of gradually larger spherical caps on the capped-cylinder model (see Figure 3A). Actually, calculations for rods with spiky decoration at their ends (not shown) exhibit similar behavior as the smoother ones reported here. Again, with just some quantitative differences the simulated spectra (Figure 3C) show the same tendency as the experimental ones (Figure 3B) (i.e., gradual damping and considerable red-shift of the LPB as the volume of the Pt cap is increased). This seems to indicate that the main effect is due to the increase in the global aspect ratio of the nanostructure, but not specifically on the geometrical details at the nanoscale. Also note that the experimental rods obtained through deposition of large amounts of Pt (right-most particle in Figure 1A) show some rough coating at the lateral edges, which has not been considered in the model.

The red-shift observed in the LPB of Figure 3 is due to a large extent to the change in aspect ratio of the particle when Pt is added to the tips. The nature of the material that is actually added seems to be less important, as long as it behaves as a good metal at the near-IR wavelengths where these bands occur. This is demonstrated in Figure 4, which compares some of the spectra of Figure 3 with those obtained for pure Au particles with the same overall shape, including the thickened ends. The positions of the plasmon bands remain approximately the same when Pt is replaced by Au, though the height of the peaks is increased and the width decreased in the process. This results from smaller absorption in Au, which can be understood by comparing the dielectric functions of both materials (e.g., $\epsilon_{Au} \approx -47 + 3.5\ i$ and $\epsilon_{Pt} \approx -22 + 40\ i$ at a wavelength of 1000 nm,[25,26] both of them large in magnitude but with ϵ_{Pt} more absorptive through its larger imaginary part). In brief, the LPB of tip-coated particles is red-shifted as either more gold or more platinum is added to the particle because of the increase in the geometrical aspect ratio, but it is broader when platinum is added instead of gold, because of larger absorption via the interband transitions noted above.

The behavior just described for the far-field extinction spectra is reflected in the near-field at the LPB wavelengths, as shown in Figure 5. This band is associated to a charge oscillation pattern with opposite charges piling up at the particle ends and giving rise to strong field enhancement. Pure gold dumbbell-like particles (Figure 5B) produce similar field enhancement as regular rods (Figure 5A) but with larger peak broadening due to stronger coupling to radiation[33] (shorter lifetime) resulting from increasing aspect ratio. When the particle tips are coated with Pt instead of Au (Figure 5C), a similar field pattern is observed as in the pure gold dumbbell but with much weaker field enhancement, consistent with the stronger absorption-driven broadening described in Figure 4B.

4. Conclusions

In summary, two different patterns of Pt-coating of Au nanorods have been analyzed consisting of either full overcoating or mass deposition at the rod ends (tip-coating). The optical behavior of our rods seems to be largely controlled by their geometrical shape profile with a dominant longitudinal band at long wavelengths that is red-shifted as the aspect ratio is increased by adding more metal to the particle. A side effect of adding Pt is to enhance absorption thus producing band broadening. The optical far-field response is rather independent

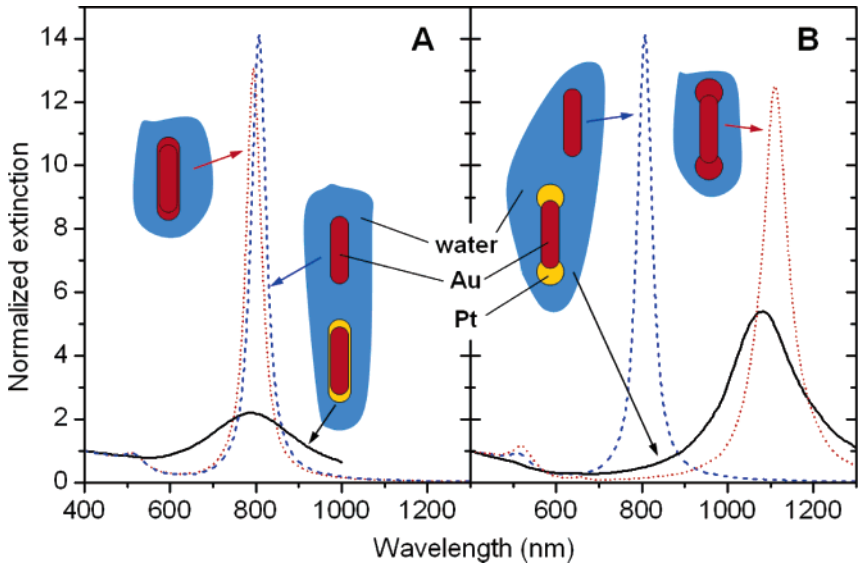

Figure 4. (A) Angle-averaged calculated extinction spectra for the pure gold rod of Figure 2 (dashed blue curve), the right-most Pt-overcoated rod of Figure 2 (solid black curve), and the same rod when gold is added instead of platinum (dotted red curve). (B) Angle-averaged calculated extinction spectra for the pure gold rod of Figure 3 (dashed blue curve), the right-most Pt-tip-coated particle of Figure 3 (solid black curve), and a particle with the same geometry as the latter but with Pt replaced by Au (dotted red curve).

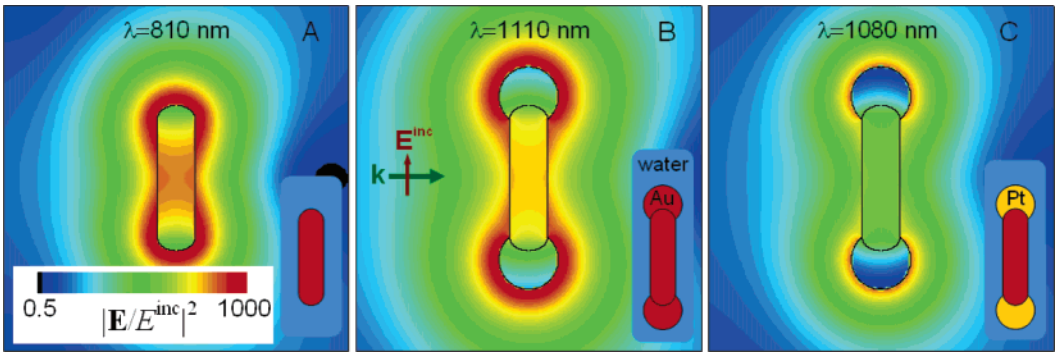

Figure 5. Near field $|\mathbf{E}|^2$ maps for longitudinal modes of regular gold nanonorods (A) and decorated gold nanorods with either more Au (B) or Pt (C) added in the tips. The log contour scale is shared across all three plots.

of finer geometrical details of the deposited Pt, the basic difference between our two kinds of particles lying on the overall Pt distribution (i.e., whether it is concentrated at the Au rod ends or uniformly distributed on the whole surface). Local roughness and small sharp features might modify significantly the near field, but they are averaged out for low-order modes for which the induced charge has a smooth envelope along the extension of the nanoparticles. From the results presented here, we find that our Pt-coated Au rods can find potential application in situations in which a broad spectral region is required, such as biosensing, where one is often interested in having sensitivity within a broad range of wavelengths, which our particles can certainly offer on demand, because the broadening of the LPB can be tuned through the amount of Pt, always maintaining a certain degree of field enhancement at the tips.

Acknowledgment. This work was supported by the European Commission through the Marie Curie Research Training Network "SyntOrbMag", Contract No. MRTNCT-2004-005567, and the Spanish Ministerio de Educación y Ciencia/FEDER projects MAT2004-02991 and NAN2004-08843-C05-03(05).

References and Notes

(1) Grzelczak, M.; Pérez-Juste, J.; Rodríguez-González, B.; Liz-Marzán, L. M. *J. Mater. Chem.* **2006**, *16*, 3946.

(2) Kreibig, U.; Vollmer, M. *Optical Properties of Metal Clusters*; Springer-Verlag: Berlin, 1996.

(3) Special issue on *Synthesis and Plasmonic Properties of Nanostructures*; Xia, Y.; Halas, N. J., Eds.; *MRS Bull.* **2005**, *30*, issue 5.

(4) Liz-Marzán, L. M. *Langmuir* **2006**, *22*, 32.

(5) Pérez-Juste, J.; Pastoriza-Santos, I.; Liz-Marzán, L. M.; Mulvaney, P. *Coord. Chem. Rev.* **2005**, *249*, 1870.

(6) Xia, Y.; Yang, P.; Sun, Y.; Wu, Y.; Mayers, B.; Gates, B.; Yin, Y.; Kim, F.; Yan, H. *Adv. Mater.* **2003**, *15*, 353.

(7) Im, S. H.; Lee, T. T.; Wiley, B.; Xia, Y. *Angew. Chem., Int. Ed.* **2005**, *44*, 2154.

(8) Millstone, J. E.; Park, S.; Shuford, K. L.; Qin, L.; Schatz, G. C.; Mirkin, C. A. *J. Am. Chem. Soc.* **2005**, *127*, 5312.

(9) Pastoriza-Santos, I.; Liz-Marzán, L. M. *Nano Lett.* **2002**, *2*, 903.

(10) Nehl, C. L.; Liao, H.; Hafner, J. H. *Nano Lett.* **2006**, *6*, 683.

(11) Link, S.; El-Sayed, M. A. *J. Phys. Chem. B.* **1999**, *103*, 8410.

(12) Ah, C. S.; Hong, S. D.; Jang, D. J. *J. Phys. Chem. B.* **2001**, *105*, 7873.

(13) Liu, M.; Guyot-Sionnest, P. *J. Phys. Chem. B*, **2004**, *108*, 5882.

(14) Huang, C. C.; Yang, Z.; Chang, H. T. *Langmuir* **2004**, *20*, 6089.

(15) Liu, M.; Guyot-Sionnest, P. *J. Mater. Chem.* **2006**, *16*, 3942.

(16) Obare, S. O.; Jana, N. R.; Murphy, C. J. *Nano Lett.* **2001**, *11*, 601.

(17) Pastoriza-Santos, I.; Pérez-Juste, J.; Liz-Marzán, L. M. *Chem. Mater.* **2006**, *18*, 2465.

(18) García de Abajo, F. J.; Howie, A. *Phys. Rev. Lett.* **1998**, *80*, 5180.

(19) García de Abajo, F. J.; Howie, A. *Phys. Rev. B.* **2002**, *65*, 115418.

(20) Sánchez-Iglesias, A.; Pastoriza-Santos, I.; Pérez-Juste, J.; Rodríguez-González, B.; García de Abajo, F. J.; Liz-Marzán, L. M. *Adv. Mater.* **2006**, *18*, 2529.

(21) Draine, B. T.; Flatau, P. J. *J. Opt. Soc. Am. A.* **1994**, *11*, 1491.

(22) Taflove, A.; Hagness, S. C. *Computational Electrodynamics: The Finite-Difference Time-Domain Method*; Artech House: Norwood, MA, 2000.
(23) Nikoobakht, B.; El-Sayed, M. A. *Chem. Mater.* **2003**, *15*, 1957.
(24) Liu, M.; Guyot-Sionnest, P. *J. Phys. Chem. B.* **2005**, *109*, 22192.
(25) Palik, E. D. *Handbook of Optical Constants of Solids*; Academic Press: New York, 1985.
(26) Johnson, P. B.; Christy, R. W. *Phys. Rev. B.* **1972**, *6*, 4370.
(27) The electromagnetic field can diverge near sharp corners separating continuous media. This is a mathematical pathology that is inherent to the assumption of local response and sharp boundaries. In the BEM, this is translated into divergences of the boundary sources near sharp corners that can cause numerical instability. In actual physical systems sharp corners do not exist, because atomic distances impose a discrete length scale. Furthermore, the assumption of local response breaks down at nonphysically small distances. By smoothing sharp corners through some rounding, these problems are solved and one finds a physical connection to the real particle behavior.
(28) Pérez-Juste, J.; Liz-Marzán, L. M.; Carnie, S.; Chan, D. Y. C.; Mulvaney, P. *Adv. Funct. Mater.* **2004**, *14*, 571.
(29) Bohren, C. F.; Huffman, D. R. *Absorption and Scattering of Light by Small Particles*; Wiley: New York, 1983.
(30) Kooij, E. S.; Poelsema, B. *Phys. Chem. Chem. Phys.* **2006**, *8*, 3349.
(31) Sau, T. K.; Murphy, C. J. *Langmuir* **2004**, *20*, 6414.
(32) The aspect ratio is defined here as the ratio between the total length (from tip to tip) and the diameter of the rod.
(33) Romero, I.; Aizpurua, J.; Bryant, G. W.; García de Abajo, F. J. *Opt. Express* **2006**, *21*, 9988.